PERSONAL BACKGROUND

# About Me

## Dev Dalmia

**AEROSPACE & MECHANICAL ENGINEERING STUDENT
USC 27'**

ddalmia@usc.edu

linkedin.com/in/devdalmia

Los Angeles, CA & Mumbai, India

## Relevant Experience

2024 - Present — **Research Assistant at California Institute of Technology**

Summer 2025 — **Concept Design Intern at Tata Advanced Systems Limited**

2024 - Present — **Engineering at USC Rocket Propulsion Laboratory**

## Hobbies & Interests

- Photography and FPV Drones
- Cooking and Trying New Food
- Sports and Outdoors

PROJECT BACKGROUND

# Drone Design

| | |
|---|---|
| **Presenter** | Dev Dalmia |
| **Date** | 19 January 2026 |
| **Professor** | Bo Cheng Jin |

### Project Motivation: The Crash

When I was younger, my first exposure to drones was a small Parrot Spider. I was obsessed with it. After only a few flights, I experimented with Return-to-Home settings without fully understanding the implications, setting the ascent height to 100 ft. The next time I triggered it, the drone climbed straight into a tree canopy and dropped nearly 15 feet, snapping an arm clean off. That moment revealed how much engineering hides inside something so simple. Later, when tasked with reverse-engineering a consumer electronic product, I chose a compact quadcopter to fully understand the structural design, material choices, electronic systems and engineering principles behind that memory - and build something that wouldn't break like mine did.


*Figure 1: DJI Mavic Mini*

**Engineering Inspiration**

Reverse-Engineering the DJI Mavic Mini Architecture

# Problem Statement

### CORE OBJECTIVE

To reverse-engineer a consumer electronic device and reconstruct its full structural and functional architecture within Siemens NX, including detailed GD&T, finite element analysis and electronics.

### The Engineering Challenge

Modern consumer products integrate complex geometries, tight tolerances, and application-specific materials, yet these elements are often hidden beneath aesthetic industrial design. The challenge is to decompose a real product into its constituent components, and recreate a manufacturable solid model that accurately reflects industry standards.

Beyond geometry, the problem extends to evaluating structural performance. This ensures that the reverse-engineered design is not merely visually accurate, but mechanically defensible through rigorous FEA validation.

### Process

1. **Geometric Decomposition**
   Deconstruct physical product into functional components and measure critical interfaces.
2. **Parametric Reconstruction**
   Rebuild solid models in NX with design intent, applying GD&T standards for dimensioning and tolerancing.
3. **Structural Validation (FEA)**
   Apply material models and boundary conditions to verify load paths and failure modes.
4. **Design Improvement**
   Identify failure points and propose engineering optimizations for future iterations.

# Project Introduction

## Objective

The primary goal was to reverse-engineer a small camera quadcopter and develop a complete digital model suitable for structural analysis and manufacturing. This process involved precise measurement, parametric CAD modeling, and material characterization.

## Key Deliverables

- Full 3D Assembly in Siemens NX
- Detailed Part & Assembly Drawings
- Finite Element Analysis of Key Components
- Electronics and Camera

## Design Reference

Modeled after a compact "dynamic" consumer camera drone found on Amazon. It features four outrunner motors, a central body housing electronics, and a forward-mounted camera.

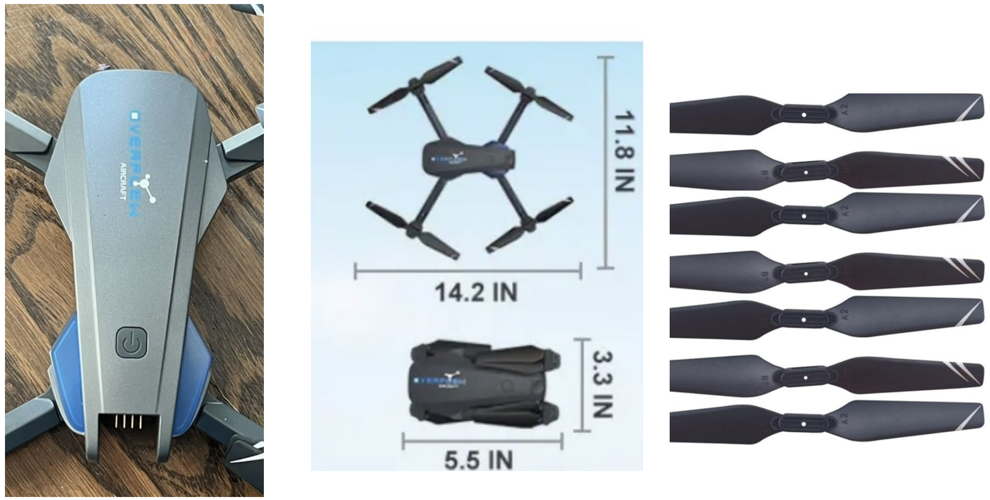


*Figure 2: Amazon Images for Basic Drone*

SYSTEM CONSTRAINTS

# Project Specifications

## PHYSICAL ENVELOPE

### 5.5" × 3.3" × 2.0"

Based on Amazon reference measurements

Comparable to size of a DJI Mavic Mini

## WEIGHT

### < 250 g

Measured Design Weight: 243 g (includes electronics)

Sub 250 g allows unregulated hobbyist operation

## CONFIGURATION

### Quadcopter

Layout: 4-Arm Radial

2 CW and 2 CCW Props in Puller Configuration

## CAD ENVIRONMENT

### Siemens NX

Units: Millimeters (mm) and Materials: PC-GF, ABS-GF

Full parametric modeling from scratch

COMPLETE CAD INTEGRATION

# Full Assembly Overview


*Figure 3: Completed NX Assembly*

SURFACE MODELING AND GD&T

# CAD Overview: Body

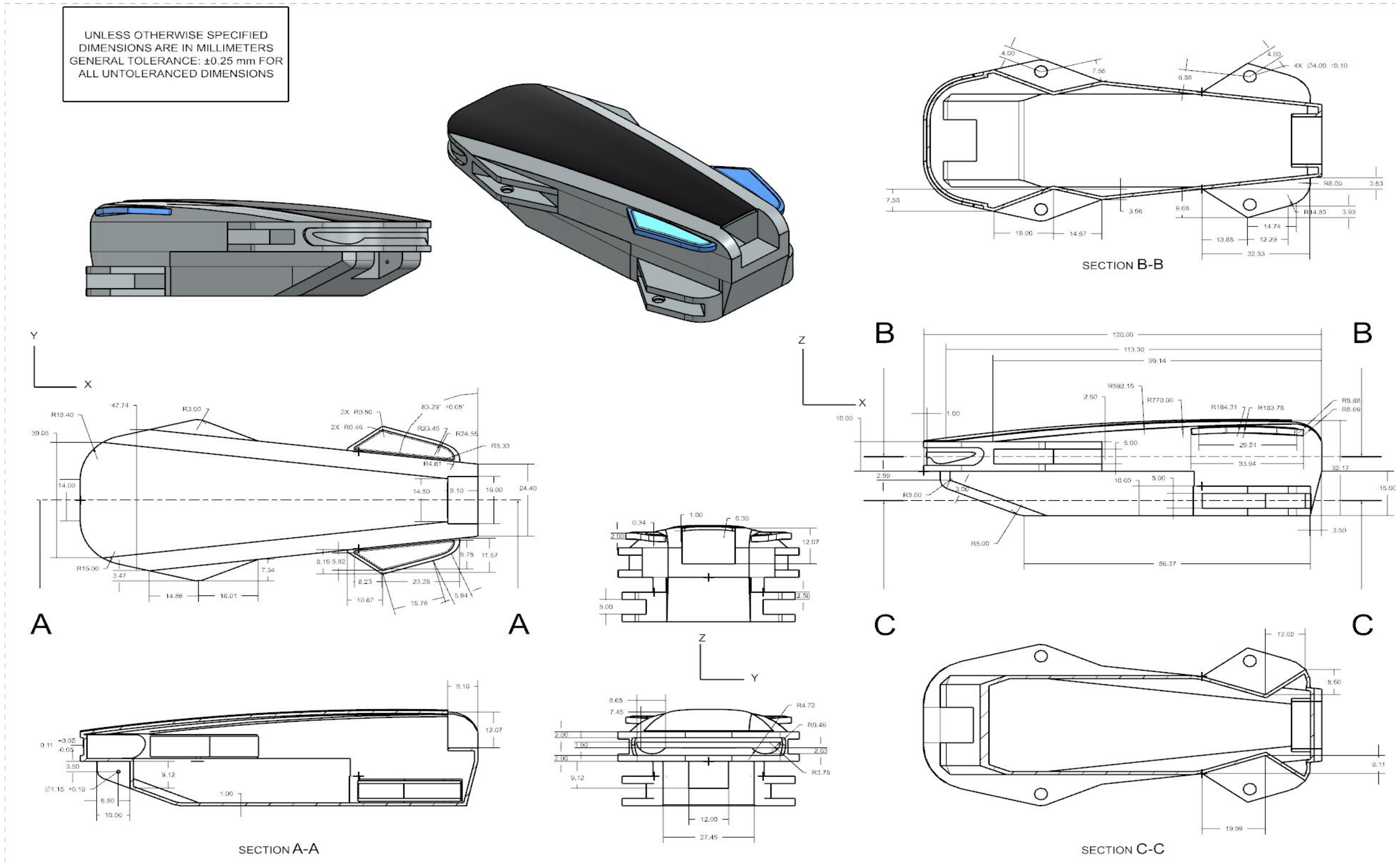


*Figure 4: Body Drawing with GD&T*

### Aerodynamic Shell

Low-profile, tapered design to minimize drag; filleted upper surfaces.

### Surface Strategy

Modeled via master sketches (XY/XZ) using extrudes, sweeps, and edge-blends.

### Integrated Mounting

Extruded arm mounts with extra space. inside of the body creates perfect arm alignment.

### GD&T Compliance

Full dimensioning ensures assembly fit with mirrored components.

# Body GD&T: Top Half

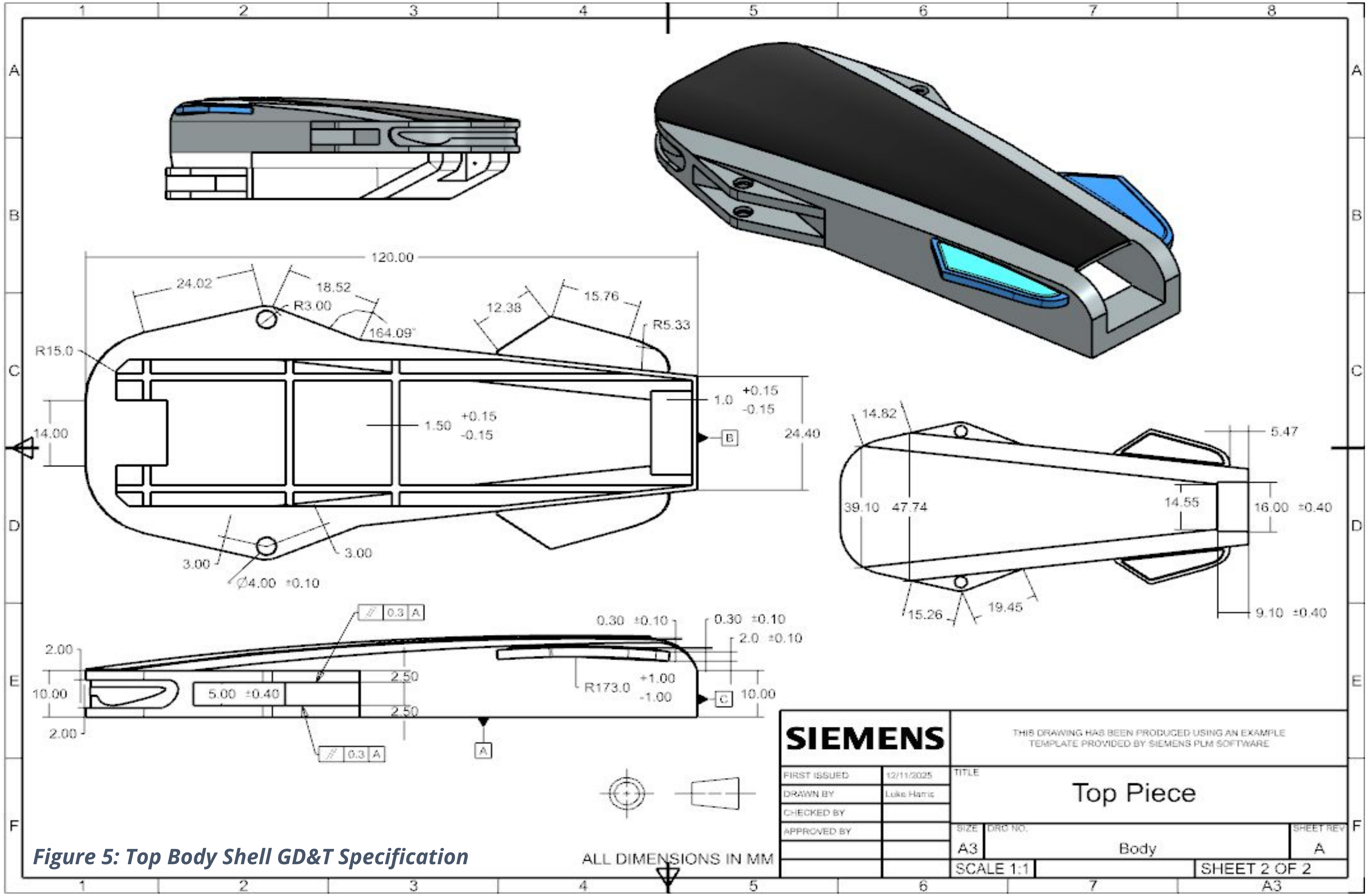


*Figure 5: Top Body Shell GD&T Specification*

### Datums A, B, C

Established main drone plains to ensure alignment with bottom shell.

### Structure

Ribs provide structural support and rigidity, and leave space for the battery.

### Perfect Fit

Toleranced surfaces for precise joints with the bottom half, arms & battery.

### Screws

Hole tolerances compensate for material shrinkage during cooling, ensuring that screws fit correctly after 3D printing.

# Body GD&T: Bottom Half

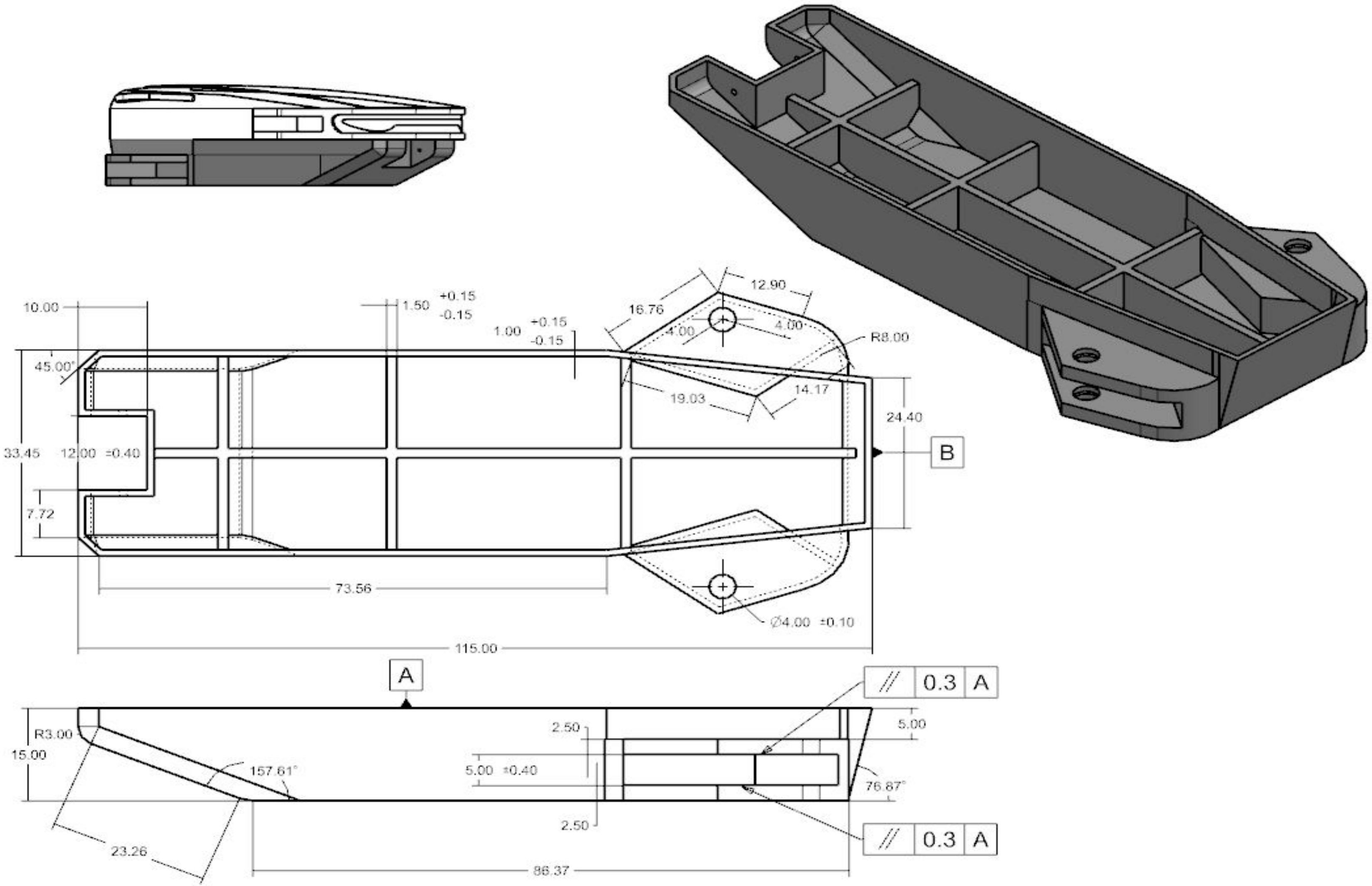


*Figure 6: Bottom Body GD&T Specifications*

### Primary Datums

Established main drone plains to ensure alignment with bottom shell.

### Structure

Ribbed sections provide structural support and rigidity, while leaving space for electronics.

### Perfect Fit

Toleranced surfaces for precise joints with the top half,  rear arms and camera.

# CAD Modeling: Propellers

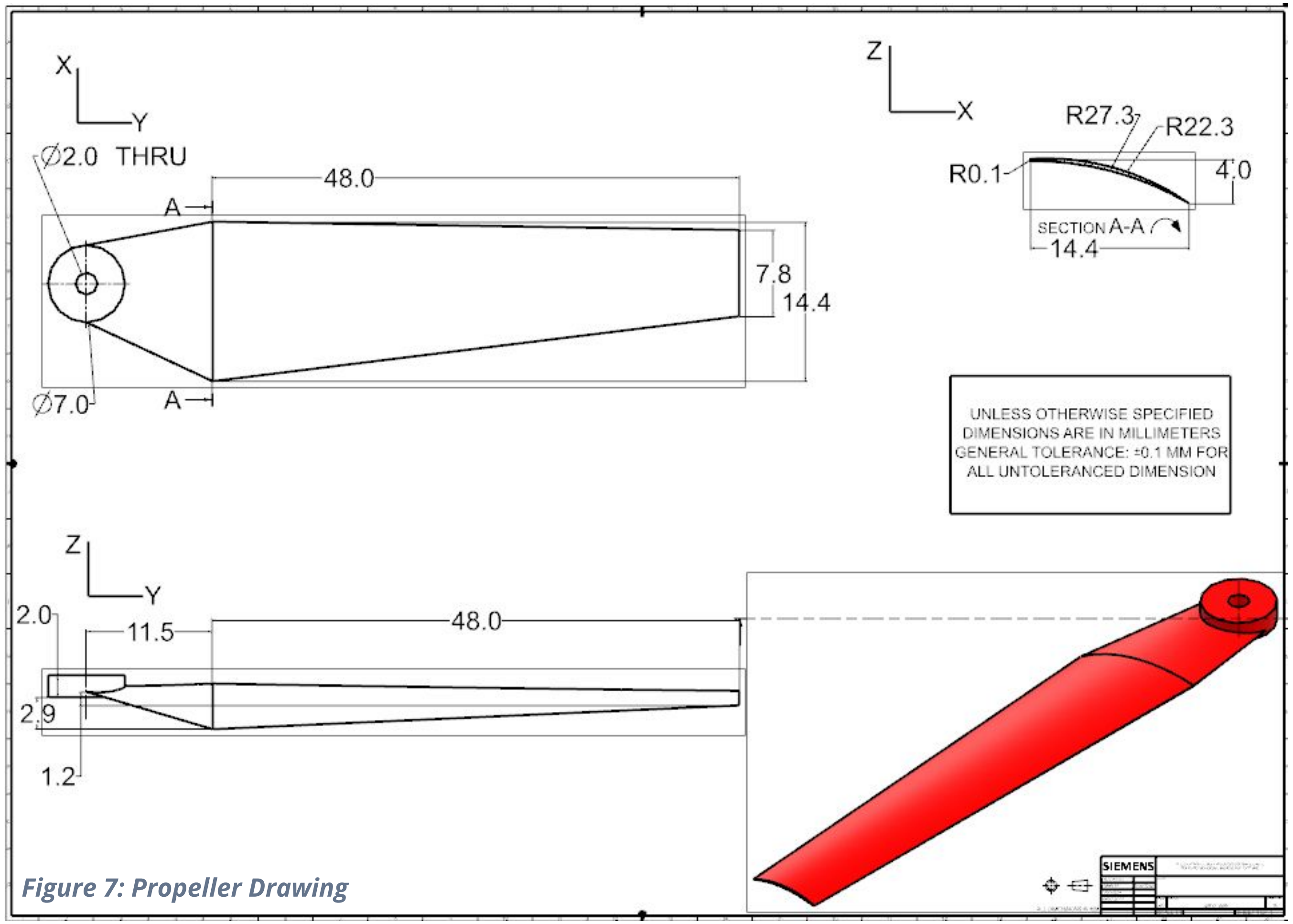


*Figure 7: Propeller Drawing*

### Geometry

Swept blade profile with twisted path for efficiency. Mirrored CW/CCW variants.

### Key Dimensions

Blade Cross-section: Swept
Hub Diameter: 8mm
Pitch: Variable Twist

### Hardware

Upper and Lower Prop Caps
Revolved Profile Clamps
Accurate Prop Assembly

### GD&T Focus

Surface profiling and concentricity constraints on hub bore

# Initial Material Choice (Insufficient Performance)

## PETG

Polyethylene Terephthalate Glycol

| 2.1 GPa | 0.35 | 1.27 g/cm³ |
| --- | --- | --- |
| YOUNG'S MODULUS | POISSON'S RATIO | DENSITY |

### Selection Rationale

PTEG is initially attractive as it is cheap, easy to print, relatively tough, and offers better heat resistance than for example PLA. However, for our drone application it has a hidden engineering failure mode as it is susceptible to creep-dominated behavior. For example, PTEG has a **viscoelastic stress-strain curve.** Under sustained loading the initial deflection looks acceptable, however excessive plastic deformation will occur under cyclic loading changing arm angels slowly and messing up thrust vectors. This is a know polymer behavior and not allowable for our drone.

### FDM Manufacturability

Printed as thin-wall shells with integrated internal features. PETG is highly printable in FDM with low warping and strong interlayer adhesion; however, its low modulus and creep behavior limit its suitability for structural drone components under sustained load.

## PA-CF

Carbon Fibre Nylon

| 5.5 GPa | 0.30 | 1.19 g/cm³ |
| --- | --- | --- |
| YOUNG'S MODULUS | POISSON'S RATIO | DENSITY |

### Selection Rationale

Carbon-Fibre Nylon is tempting as is is extremely stiff along its fiber direction, offers minimal creep, and is professionally used in aerospace applications. PA-CF's critical failure occurs in our drone application as it behaves like a **layered composite rather** than an isotropic material. It is very strong in plane but very weak between layers. In addition to this **crack propagation is sudden and catastrophic.** PA-CF does not yield well and does not absorb energy well. It optimizes stiffness at the expense of survivability which is the wrong trade in this system.

### FDM Manufacturability

PA-CF prints with high in-plane stability but requires strict moisture control, hardened tooling, and careful orientation to manage anisotropic layer bonding and maintain dimensional repeatability.

# Continued Material Choice & Manufacturability

## ABS-GF

Body & Enclosure

Glass-Filled Acrylonitrile Butadiene Styrene

| 3 GPa | 0.35 | 1.05 g/cm³ |
|---|---|---|
| YOUNG'S MODULUS | POISSON'S RATIO | DENSITY |

### Selection Rationale

ABS-GF is selected for the body and enclosure due to its **low density** and **compliant stress–strain response in thin-walled geometries**. It provides adequate stiffness for structural integrity while retaining ductility for snap-fit clips and integrated bosses to flex without brittle failure during assembly or impact. Its predictable shrinkage and strong interlayer adhesion in enclosed FDM printing enable accurate large-area shells with internal ribs and impact-tolerant protection of internal electronics.

### FDM Manufacturability

Printed as thin-wall shells with integrated internal features. ABS-like filament provides excellent printability with moderate shrinkage, enabling accurate snap-fit clips and bosses.

## PC-GF

Arms & Propellers

Glass-Filled Polycarbonate

| 4 GPa | 0.35 | 1.20 g/cm³ |
|---|---|---|
| YOUNG'S MODULUS | POISSON'S RATIO | DENSITY |

### Selection Rationale

Reserved for structural arms and rotating components where stiffness and dimensional stability are critical. PC-GF, with a flexural modulus of approximately **4.0 GPa**, provides high bending stiffness while maintaining consistent interlayer toughness in FDM printing. Compared to PA-CF (≈ **5–6 GPa** in-plane modulus), PC-GF offers sufficient stiffness for load-bearing arms without the pronounced anisotropy, interlayer brittleness, and impact-sensitive failure modes associated with carbon-fiber-reinforced nylons, resulting in more reliable manufacturability and crash tolerance.

### FDM Manufacturability

Printed at higher temperatures to realize 4 GPa stiffness. Requires careful layer adhesion control to maintain slender geometries and thin airfoil sections without warping or creep.

MATERIAL COST BENEFIT ANALYSIS

# Final Filament Cost Comparison

| Material | Filament Name | Price ($/kg) | Supplier | Notes |
|---|---|---|---|---|
| PETG | PETG Basic | $30.00 | Generic (Amazon, Micro Center) | Baseline engineering filament |
| ABS-GF | Glass Fibre ABS | $28.99 | Bambu Lab | Glass-fibre reinforced ABS |
| PC-GF (PA6-GF) | Glass Fibre PC | $59.99 | Bambu Lab | Glass-fibre reinforced engineering polymer |
| PA-CF (PA6-CF) | Carbon Fibre PC | $79.99 | Bambu Lab | Carbon-fibre reinforced nylon |

Data sourced from major suppliers as of current market rates.

# Manufacturing

## 3D Printing Approach

**Phase 1 - FDM Print Strategy**

- **Print Orientation:**

Parts are oriented so primary loads act **within the XY plane**, where layer strength and fiber alignment are highest. This minimizes Z-axis tensile stresses, which are the weakest failure mode in FDM. Correct orientation directly improves stiffness, impact resistance, and fatigue life.

- **Layer Height Selection**

Layer heights of **0.25–0.30 mm** are used with a **0.6 mm nozzle** to maximize interlayer diffusion and fiber bonding. Thinner layers reduce thermal bonding; thicker layers reduce dimensional accuracy and consistency.

- **Perimeter and Wall Strategy**

Structural strength is concentrated in **4–6 continuous perimeters**, not infill. Thick outer walls resist crack initiation, absorb impact energy, and carry bending loads more effectively than increasing infill density.

- **Infill Geometry and Density**

**Gyroid or cubic infill** is used to maintain isotropic stiffness without stress risers. Density is set to **15–25% for ABS-GF body components** and **30–40% for PC-GF arms** to balance stiffness and weight.

- **Thermal Control and Enclosure Management**

Chamber temperatures are maintained at **45–60 °C for ABS-GF** and **60–70 °C for PC-GF** to reduce thermal gradients, prevent warping, and improve interlayer adhesion. Open-air printing is avoided for all structural parts.

- **Moisture Control**

PC-GF filament is dried at **80–90 °C for 6–8 hours** and maintained below **0.1% moisture content** during printing. Moisture contamination causes foaming, fiber pullout, and reduced mechanical strength.

# Manufacturing

## Assembly + Repeatability

Glass-Filled Polycarbonate

**Phase 2 - Post-Print Processing, Assembly, and Validation Workflow**

- **Controlled Cool-Down and Stress Relief**

Printed parts remain in the heated enclosure until temperature falls below **40 °C** to minimize residual stress and prevent delayed warping. Controlled cool-down improves dimensional stability and fatigue resistance, especially in glass-filled polymers.

- **Support Removal and Edge Conditioning**

Supports are removed while parts are between **30–40 °C** to reduce brittleness. Supports are cut rather than snapped to avoid introducing microcracks that can propagate under vibration and cyclic thrust loading.

- **Heat-Set Insert Installation**

Heat-set inserts are installed only at high-cycle locations (arm mounts, motor mounts). Inserts are pressed at material-specific temperatures to prevent polymer degradation and preserve fiber alignment in the surrounding matrix.

- **Dimensional Verification and Tolerance Control**

Critical datum surfaces, arm mounting interfaces, and motor faces are measured to a functional tolerance of **±0.2 mm**. Maintaining positional accuracy is essential for thrust alignment, vibration minimization, and control stability.

- **Vibration and Spin-Up Testing**

Motors are incrementally spun up first without, then with propellers to identify resonant frequencies and imbalance. Audible layer buzz or harmonic vibration is used as an indicator of poor layer adhesion or internal delamination.

- **Flight Readiness Confirmation**

A component passes flight readiness only if dimensional accuracy, thermal stability, vibration response, and load symmetry meet predefined acceptance criteria. Parts showing asymmetry, creep, or resonance are rejected prior to flight

# Real World Testing

**Motivation:** FDM polymers are anisotropic and process-dependent; datasheet properties do not represent printed part behavior

**Method:** Instron uniaxial tensile and flexural tests on printed coupons in representative orientations

**Data extracted:** Elastic modulus, yield behavior, failure strain, and load–deflection stiffness

**Key result:** PETG showed time-dependent creep; glass-fiber-reinforced polymers exhibited higher stiffness and dimensional stability

**Design impact:** Replaced nominal material values with experimentally measured properties in FEA

**Outcome:** PC-GF arms for stiffness and creep resistance; ABS-GF body for impact tolerance and ductility

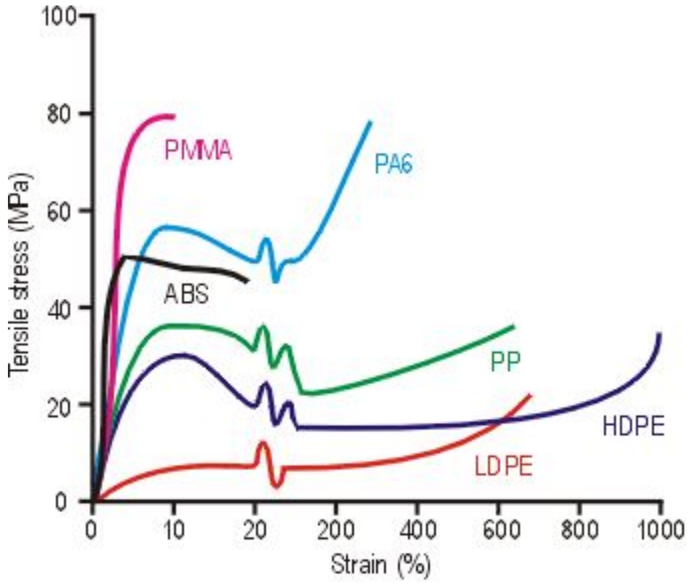


PRODUCTION EXPECTATIONS

# Assembly

## Global Reference Frame

The main body is fixed at the global XYZ origin (0,0,0). All subsequent components (arms, battery, camera) are positioned relative to this central body's datums. This ensures symmetry about the Y-axis and simplifies downstream FEA boundary definitions.

## Constraint Hierarchy

Arms: Locked via concentric hinge constraints and planar mates between the arm base and body pads.

Battery & Camera: Mated to internal cavity planes and front datum surfaces for precise fitment.

Hardware: Screws aligned concentrically with mounting holes; heads mated to external faces.

## Degrees of Freedom

Propellers are constrained concentrically to the motor boss and mated to the boss face, leaving the axial rotation free. This specifically preserves the intended rotational motion for kinetic visualization.

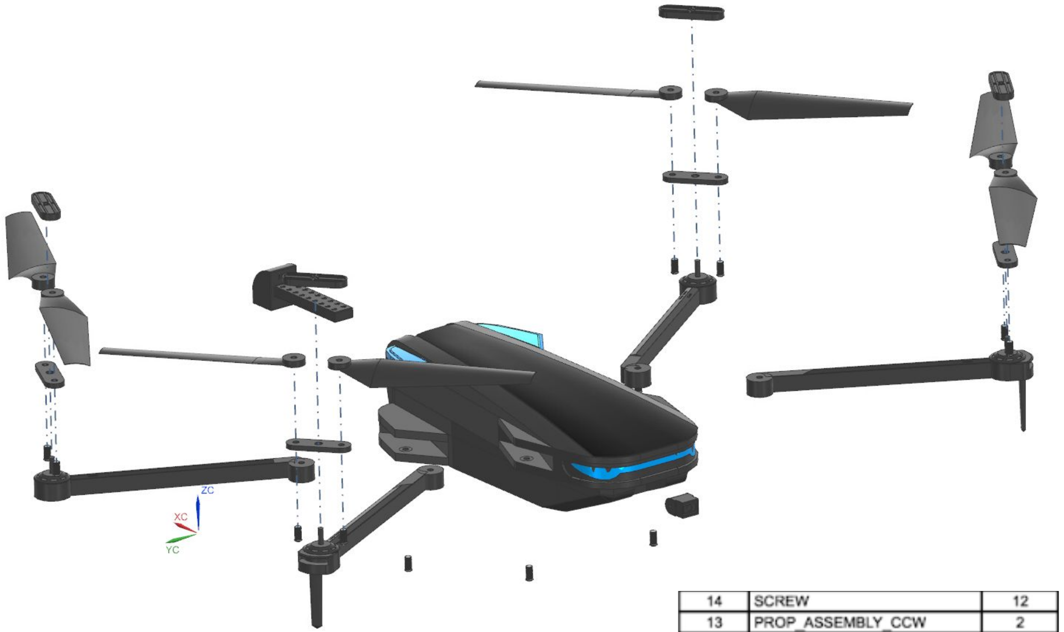


| PC NO | PART NAME | QTY |
|---|---|---|
| 14 | SCREW | 12 |
| 13 | PROP_ASSEMBLY_CCW | 2 |
| 12 | PROP_CCW | 4 |
| 11 | PROP_ASSEMBLY_CW | 2 |
| 10 | PROP_CAP_BOTTOM | 4 |
| 9 | PROP_CW | 4 |
| 8 | PROP_CAP_TOP | 4 |
| 7 | FRONT_RIGHT_ARM | 1 |
| 6 | FRONT_LEFT_ARM | 1 |
| 5 | REAR_LEFT_ARM | 1 |
| 4 | REAR_RIGHT_ARM | 1 |
| 3 | BATTERY | 1 |
| 2 | CAMERA | 1 |
| 1 | BODY | 1 |

*Figure 8: Exploded Assembly with Bill of Materials*

# Bill of Materials

| Part / Subsystem | Material | Qty | Unit Mass (g) | Total Mass (g) | Est. Unit Price ($) | Est. Total Price |
|---|---|---|---|---|---|---|
| Main Body Shell | ABS-GF | 1 | 35.21 | 35.21 | $3.00 | $3.00 |
| Front Arms | PC-GF | 2 | 15.28 | 30.56 | $4.00 ea | $8.00 |
| Back Arms | PC-GF | 2 | 12.73 | 25.46 | $3.50 ea | $7.00 |
| 2 Blade Propellers | PC-GF | 8 | 2.14 | 17.12 | $1.00 ea (typical micro props set pricing) | $8.00 |
| Propeller Caps | PC-GF | 8 | 1.3 | 10.4 | $0.75 ea (small 3D-printed caps) | $6.00 |
| Battery | 3S ~650mAh LiPo (Tattu) | 1 | 45 | 45 | $11.50 (Tattu 3S 650mAh is ≈ $10–13) (Amazon) | $11.50 |
| Motors | Metal (Happymodel EX1202.5 8000 KV) | 4 | 5 | 20 | $16.00 ea (≈ $15.99 current price) (Pyrodrone) | $64.00 |
| Flight Controller + ESC Stack | Mixed metals/PCB | 1 | 13.5 | 13.5 | $70.00 (SpeedyBee F405 Mini stack typically $60–77) (Speedy Bee) | $70.00 |
| Wiring | Copper + Silicone + XT30 | 1 | 10 | 10 | $5.00 (XT30 pigtail + misc. wire) | $5.00 |
| FPV Camera | RunCam Nano 3 | 1 | 1.1 | 1.1 | $24.00 (≈ $23.99 retail) (RaceDayQuads) | $24.00 |
| Radio Receiver | FrSky R-XSR | 1 | 1.5 | 1.5 | $23.00 (≈ $21.8–24.99 typical) (Rotor Riot Store) | $23.00 |
| Video Transmitter | TBS Unify Pro 32 Nano | 1 | 1 | 1 | $30.00 (≈ $29.95–37.99) (weBLEEDfpv) | $30.00 |
| Screws (M2 6061 Al.) ★ | 6061-T6 Al | 12 | 1.08 | 12.96 | $0.05 ea (bulk hardware) | $0.60 |
| Micro GPS | BN-220 module | 1 | 5.3 | 5.3 | $20.00 (BN-220 modules ≈ $18–20) (SKYZONEFPV) | $20.00 |
| Total | | | | 233.32 | | $280.10 |

STRUCTURAL ANALYSIS SETUP

# FEA Component Selection

## Target Component: Front-Right Arm

For the Finite Element Analysis (FEA), we selected the front-right arm. As the primary load path between the propulsion system and the central body, this component acts as a cantilever beam and is critical for structural integrity.

## Load Transmission

The arm has an 71 mm lever arm that carries the full motor thrust, along with the weight of the propeller, prop cap, and motor. These loads generate significant bending moments at the root during operation.

## Criticality Rationale

Being slender compared to the central body, the arms are expected to sustain the majority of structural deflection. Ensuring this member can withstand flight maneuvers (3:1 thrust) and minor impacts validates the safety of the entire drone.

*Figure 9: Mesh Density of Arm*

# FEA Loading Conditions

### DESIGN MASS

## 250 g (0.2 kg)

Measured: 233 g (Components)
Includes allowance for electronics & wiring

### PERFORMANCE TARGET

## 3 : 1 Ratio

Goal: Dynamic Camera Drone
High maneuverability (Climb/Accelerate)

### OPERATIONAL THRUST

## 1.8 N / Motor

Hover Load: ~0.49 N per arm
Max operational thrust per arm

### FOS DESIGN LOAD

## 5.5 N / Motor

Safety Factor: 3.0×
Applied conservatively to account for impact

ANALYTICAL VERIFICATION

# Hand Calculations for Arms

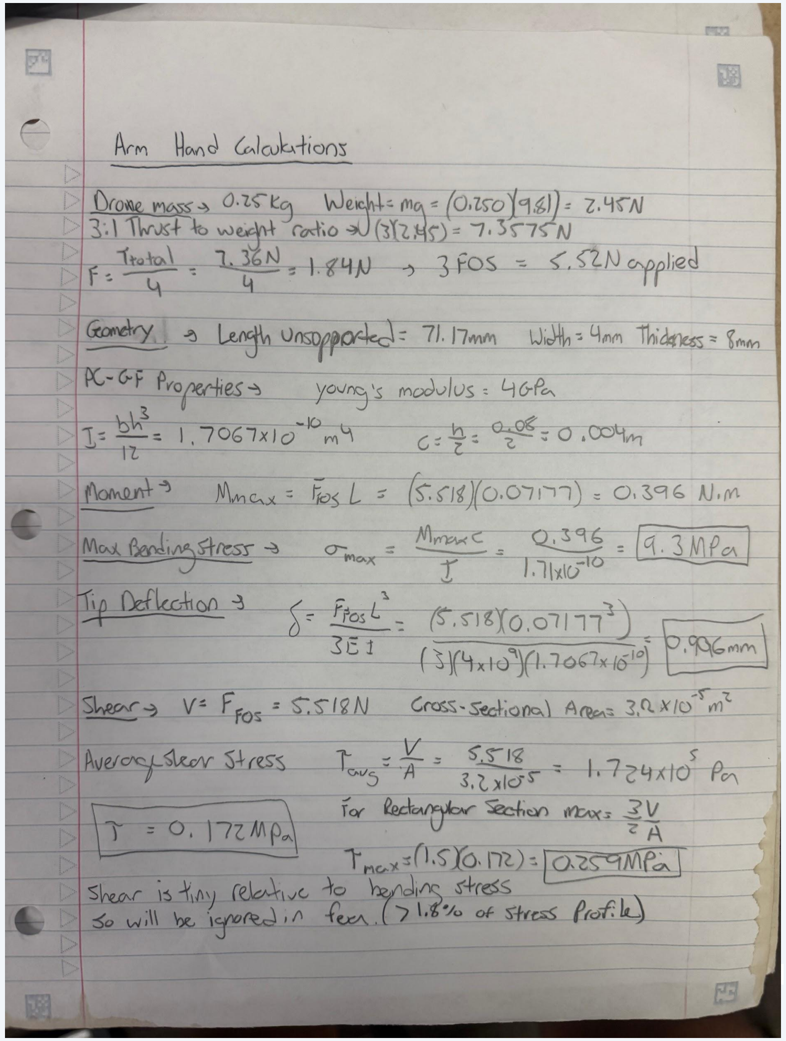

Arm Hand Calculations

Drone mass → 0.25 kg Weight = mg = (0.250)(9.81) = 2.45N

3:1 Thrust to weight ratio → (3)(2.45) = 7.3575 N

$F = \frac{T_{total}}{4} = \frac{7.36N}{4} = 1.84N$ → 3 FOS = 5.52N applied

Geometry → Length Unsupported = 71.17mm Width = 4mm Thickness = 8mm

PC-GF Properties → young's modulus: 4GPa

$I = \frac{bh^3}{12} = 1.7067\times10^{-10}\ m^4$ $c = \frac{h}{2} = \frac{0.008}{2} = 0.004m$

Moment → $M_{max} = F_{fos} L = (5.518)(0.07177) = 0.396$ N.m

Max Bending Stress → $\sigma_{max} = \frac{M_{max} c}{I} = \frac{0.396}{1.71\times10^{-10}} =$ 9.3 MPa

Tip Deflection → $\delta = \frac{F_{fos} L^3}{3EI} = \frac{(5.518)(0.07177^3)}{(3)(4\times10^9)(1.7067\times10^{-10})} =$ 0.906mm

Shear → $V = F_{fos} = 5.518N$ Cross-Sectional Area = $3.2\times10^{-5}\ m^2$

Average Shear Stress $\tau_{avg} = \frac{V}{A} = \frac{5.518}{3.2\times10^{-5}} = 1.724\times10^5$ Pa

$\tau$ = 0.172 MPa

For Rectangular Section max = $\frac{3V}{2A}$

$\tau_{max} = (1.5)(0.172) =$ 0.259 MPa

Shear is tiny relative to bending stress so will be ignored in fea. (>1.8% of stress profile)

### MAX BENDING MODULUS

Mmax = P · L
= 0.396 Nm

| | |
|---|---|
| P (Load) | 5.6 N |
| L (Length) | 71.2 mm |

### FLEXURAL STRESS

σ = (M · c) / I
= 9.3 MPa

| | |
|---|---|
| c (Centroid Dist.) | h / 2 |
| I (Moment of Inertia) | Geometry Dependent |

### MAX DEFLECTION

δmax = (P · L3) / (3 · E · I)
= 0.906mm

| | |
|---|---|
| E (Modulus) | 4,000 MPa (PC-GF) |

SETUP AND CONSTRAINTS

# FEA Boundary Conditions

## Fixed Support (Root)

The pivot joint at the root of the arm is modeled as a fixed support. All translations (X, Y, Z) and rotations are fully constrained to simulate the rigid fastening of the arm to the central drone body.

## Load Application

The 5.6 N design load is applied as a distributed pressure over the motor-mount face. This method approximates how thrust is transmitted through the motor mounting plate and screws, rather than applying an unrealistic point load on a single node.

## Mesh Strategy

A 3D tetrahedral mesh was generated with local refinement applied to critical high-stress regions, specifically the motor-mount boss and the fillet transition near the root.

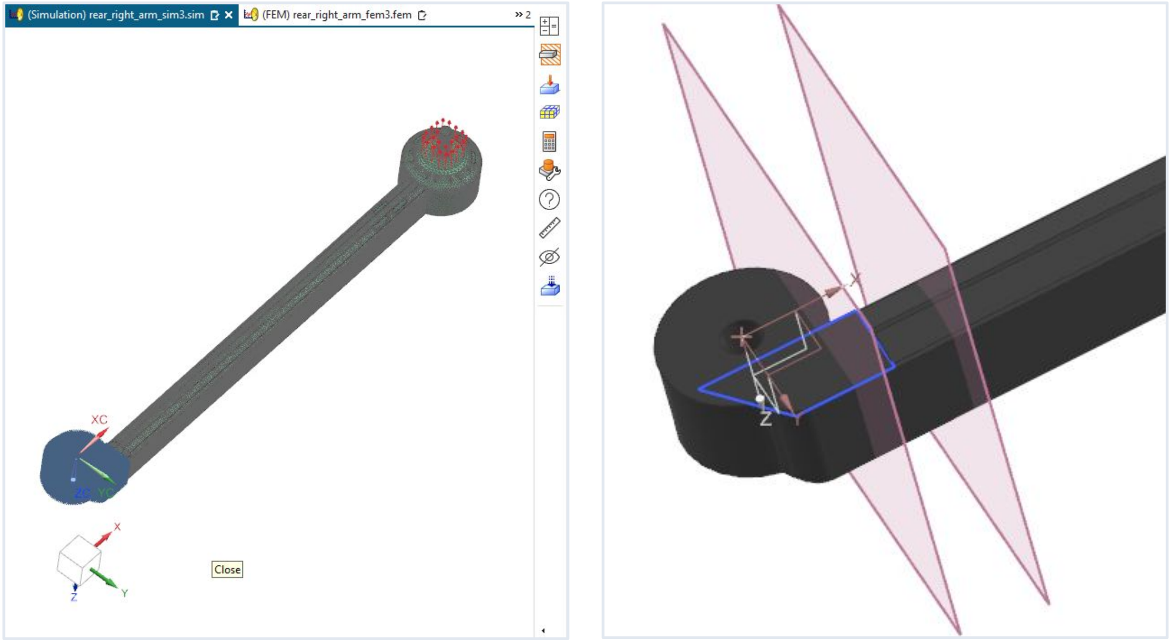


*Figure 10: Force Application on Arm Distributed over Motor Plate*

DESIGN OPTIMIZATION

# FEA Geometry Refinement

**ITERATION 1** — **Initial Geometry**

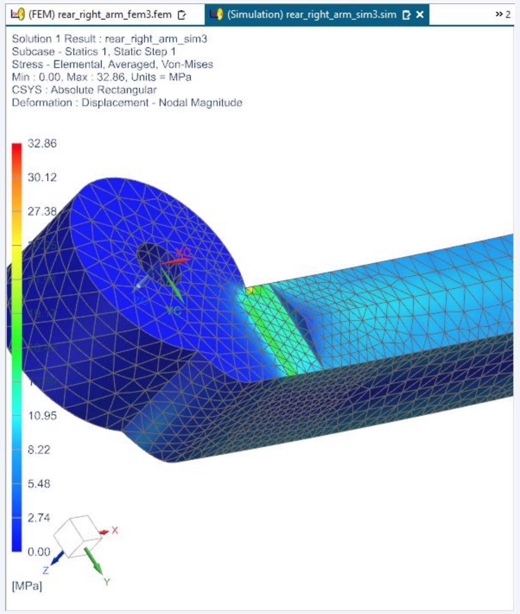


**Peak Stress** ~32 MPa

Initial uniform cross-section with sharp corners at the root interface. High stress concentrations observed at the fixed support boundary due to singularity effects.

**ITERATION 2** — **Edge Blend**

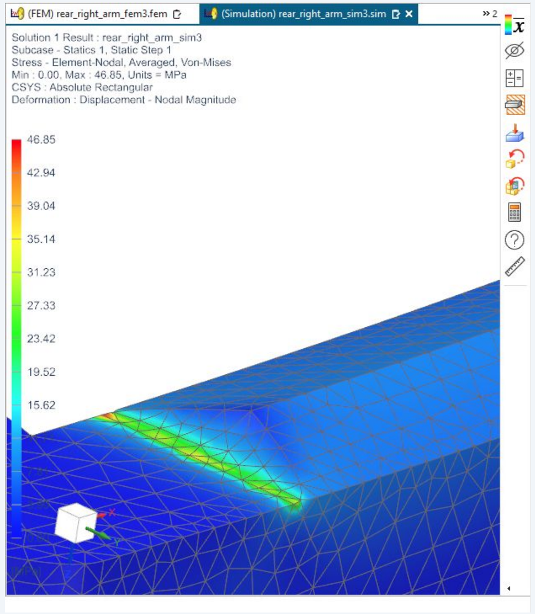


**Peak Stress** ~47 MPa

Added 1.5mm fillet radii at the root and motor boss transitions. Stress distribution improved but localized peaks remain near the constrained boundary nodes.

**FINAL** — **Fillet + Increased Edge Blend**

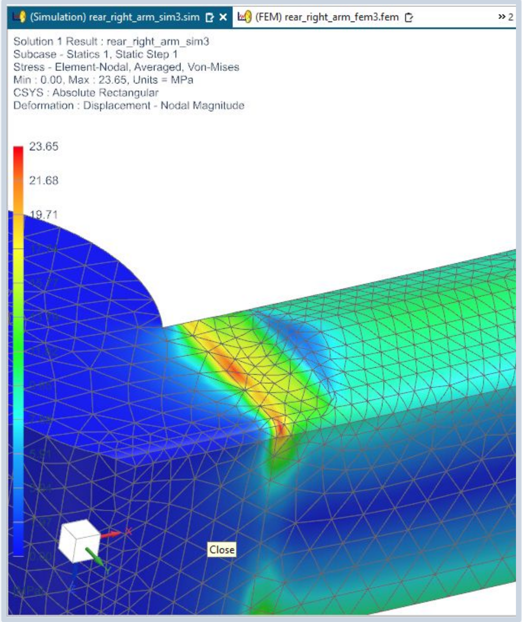


**Peak Stress** ~24 MPa

Implemented tapered beam profile increasing section depth at root. Stress gradients smoothed significantly, with peak stress stabilized well below yield strength.

MESH REFINEMENT STUDY

# FEA Convergence: 1st & 2nd

### Comparative Analysis

Geometry V1 exhibits partial convergent behavior in peak stress due to the singularity at the sharp re-entrant corner; stress continues to rise significantly with mesh refinement. Geometry V2 introduces a 2mm fillet, resulting in a more stable convergence however the unaveraged stress continues to rise with finer meshes.

| Ele Size (mm) | No. of Ele | No. of Nodes | Max Disp | unAve Stress | Ave Stress | Delta unAve | Delta Ave |
|---|---|---|---|---|---|---|---|
| 1.5 | 14302 | 25307 | 1.689 | 30.11 | 19.83 | -3.24 | -0.01 |
| 1 | 28686 | 48393 | 1.69 | 26.87 | 19.82 | 13.34 | 13.04 |
| 0.75 | 50572 | 82590 | 1.691 | 40.21 | 32.86 | 22.3 | 1.54 |
| 0.5 | 126773 | 197118 | 1.692 | 62.51 | 34.4 | 7.65 | 16.42 |
| 0.25/1 | 101311 | 158622 | 1.692 | 70.16 | 50.82 | 9.65 | 5.72 |
| 0.2/1 | 136346 | 209188 | 1.692 | 79.81 | 56.54 | | |

| Ele Size (mm) | No. of Ele | No. of Nodes | Max Disp | unAve Stress | Ave Stress | Delta unAve | Delta Ave |
|---|---|---|---|---|---|---|---|
| 1.5 | 14258 | 25233 | 1.263 | 42.18 | 20.67 | -1.13 | 17.47 |
| 1 | 29192 | 49242 | 1.264 | 41.05 | 38.14 | 25.26 | 8.71 |
| 0.75 | 50823 | 83017 | 1.265 | 66.31 | 46.85 | 19.02 | 3.17 |
| 0.5 | 126989 | 197320 | 1.267 | 85.33 | 50.02 | 6.16 | 15.1 |
| 0.25/1 | 101014 | 158488 | 1.271 | 91.49 | 65.12 | 13.36 | -8.17 |
| 0.2/1 | 137371 | 210988 | 1.268 | 104.85 | 56.95 | | |

### Stress Convergence Comparison (V1 vs V2)

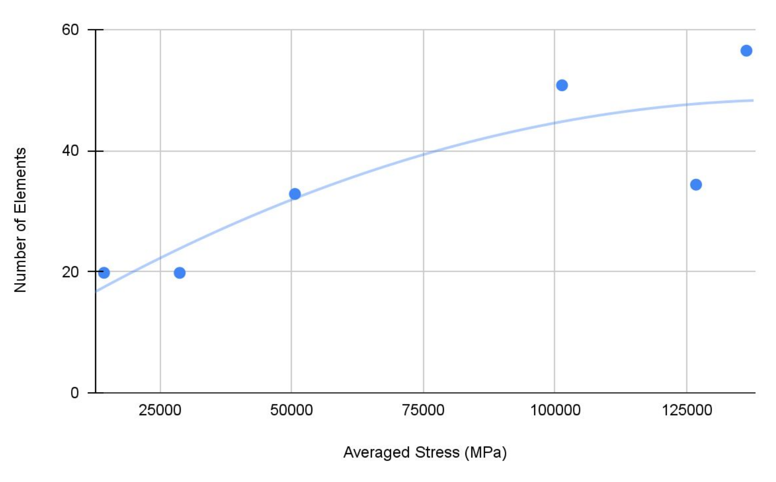


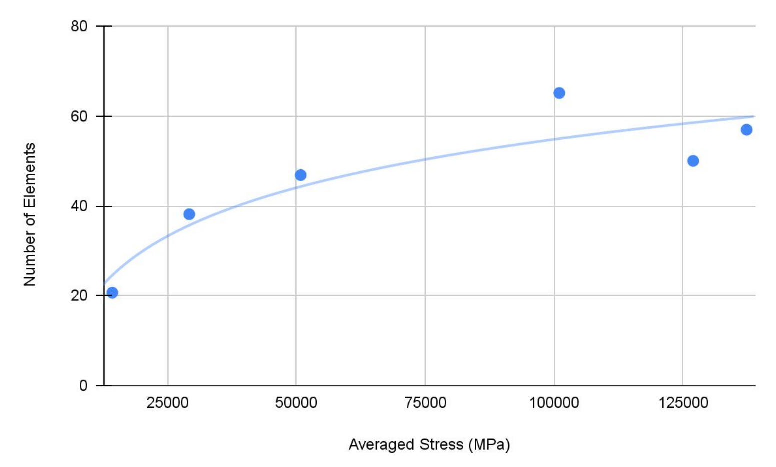

MESH REFINEMENT STUDY

# FEA 3rd Mesh Convergence

### Convergence Conclusion

Displacement convergence: Maximum displacement stabilizes at 1.496 → 1.516 mm, with <0.3% change between the two finest meshes, indicating fully converged global stiffness behavior.

Stress convergence: Averaged stress increases smoothly 12.30 → 21.16 MPa with mesh refinement, with ~3.0% change between the two finest meshes, demonstrating convergence of the stress field.

Linearity agreement: The near-linear relationship between averaged stress and node count over the refinement range indicates consistent numerical behavior and absence of mesh-induced artifacts.

| Ele Size (mm) | No. of Ele | No. of Nodes | Max Disp | unAve Stress | Ave Stress | Delta unAve | Delta Ave |
|---|---|---|---|---|---|---|---|
| 1.5 | 15343 | 26873 | 1.496 | 21.39 | 12.3 | 2.37 | 0.06 |
| 1 | 29565 | 50026 | 1.496 | 23.76 | 12.36 | 7.91 | -1.24 |
| 0.75 | 52092 | 83319 | 1.497 | 31.67 | 13.21 | 6.67 | -5.45 |
| 0.5 | 130987 | 198453 | 1.500 | 38.34 | 20.03 | 1.22 | 2.65 |
| 0.25/1 | 102651 | 158621 | 1.512 | 39.56 | 20.54 | 3.87 | -3.87 |
| 0.2/1 | 137562 | 210786 | 1.516 | 43.43 | 21.16 | | |

### Stress vs. Node Count (4.5N Load)

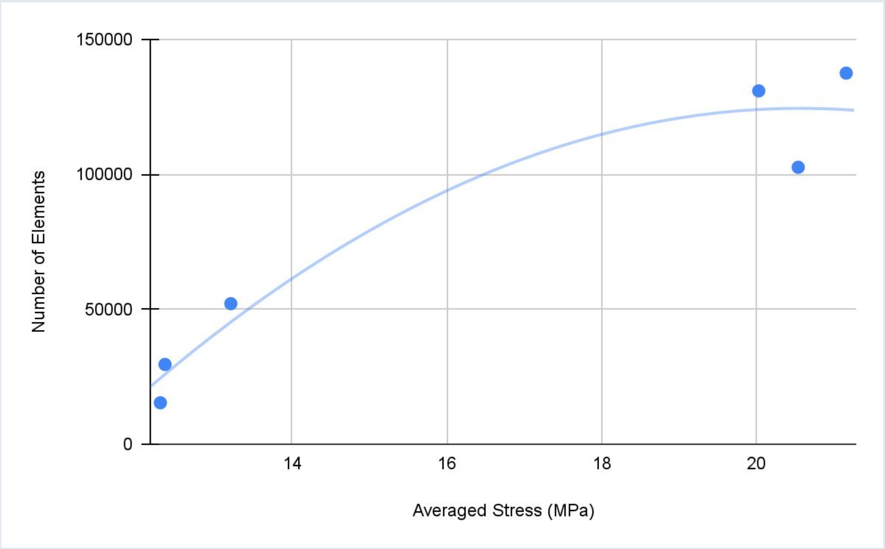

# Additional Load Factors: Wind & Vibration

Wind & Vibration Calc

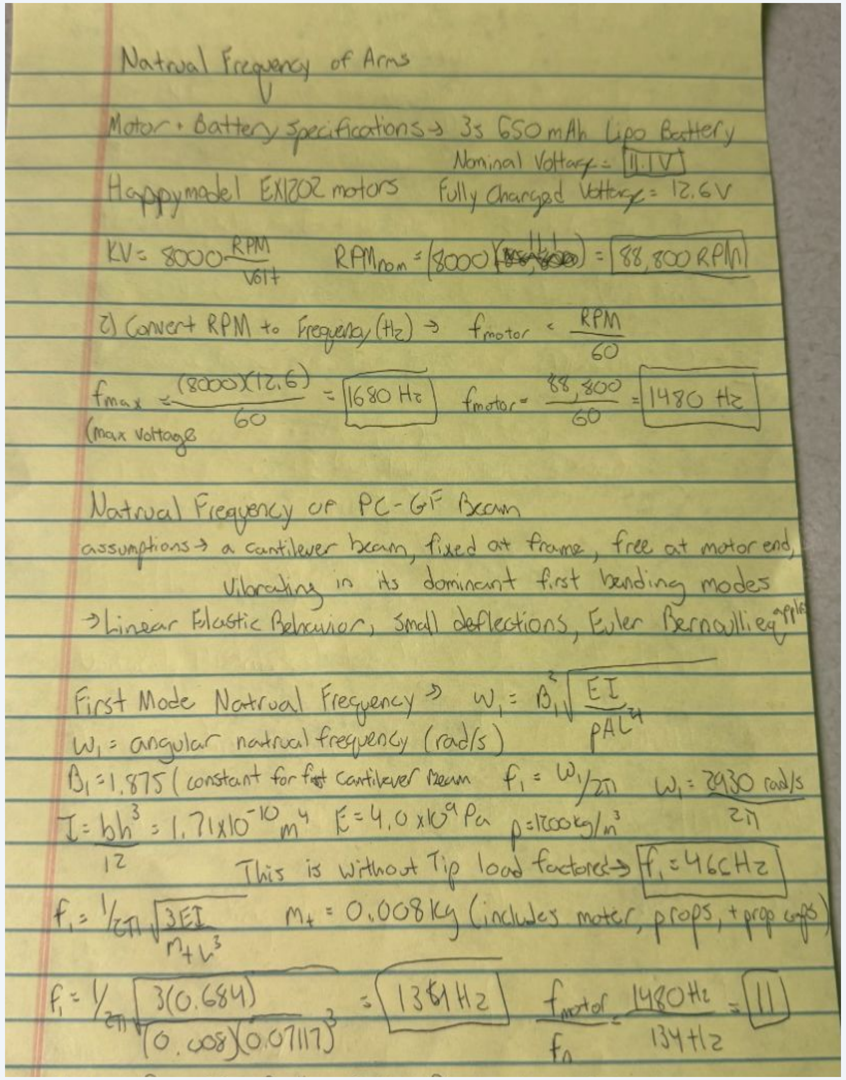


Natural Frequency Calc

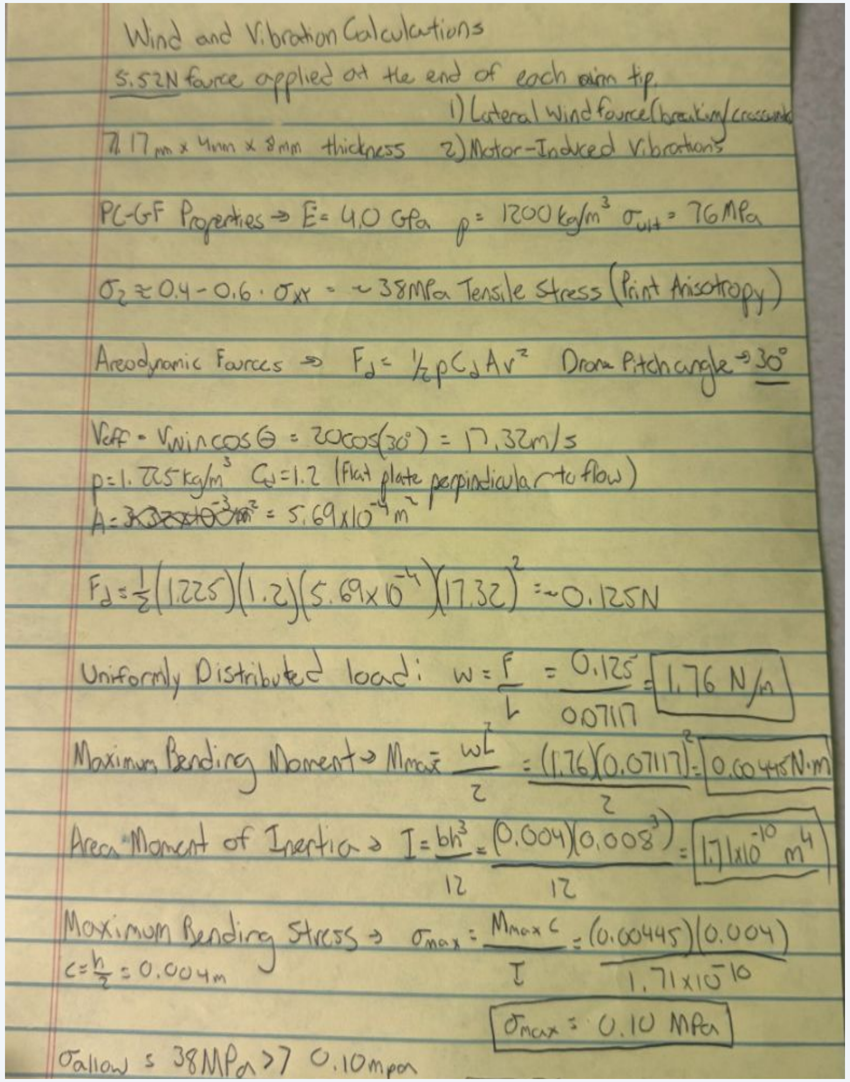


**NAT. FREQ (MODE 1)**

$\omega_1 = \beta_1^2 \sqrt{EI/\rho A L^4}$

$\beta_1$: mode constant

**FREQUENCY (HZ)**

$f = (1/2\pi) \sqrt{3EI/ML^3}$

Cantilever fundamental approx.

**AERODYNAMIC DRAG**

$F_d = \frac{1}{2} \rho C_d A v^2$

Drag force calculation.

STRUCTURAL ANALYSIS

# FEA Displacement Results

## Maximum Displacement

Under the conservative design load of 5.6 N (3× safety factor), the finite element model predicts a maximum tip displacement of 1.52 mm. This occurs at the motor mount tip, 71.2 mm from the fixed pivot.

## Strain Analysis

With an arm span of 71.2 mm, the 1.52 mm deflection corresponds to approximately 2.1% of the span.

## Material Validation

The selected material, PC-GF, has a flexural strain at break of 5.6%.

## Operational Context

At realistic operational thrust (~1.5 N), deflection scales linearly to just ~1% of the arm length, ensuring the arm remains stiff enough for precise flight control without elastic instability.

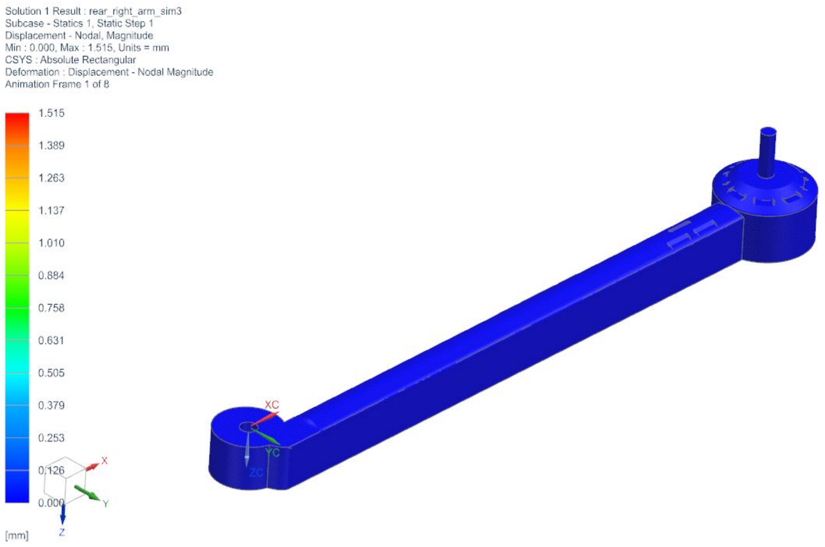


*Figure 11: Displacement of Arm under 5.6N load (0.2/1 mm Mesh)*

| Parameter | Value | Status |
|---|---|---|
| Calculated Strain (4.5N) | ~2.1% | ✓ Safe |
| Material Limit | 5.6% | |
| In-Service Est. (1.5N) | ~0.8% | ✓ Safe |

# FEA Stress Results

## Maximum Stress

Under the conservative 5.6 N design load (3× safety factor), the maximum von Mises stress reaches approximately 21.16 MPa.

> At realistic operational thrust (~1.5 N), the stress is only ~4 MPa, well within the elastic limit.

## Critical Regions

Primary Peak: Located at the root fillet where the arm blends into the hub (geometric stress concentration).

A Face Blend, Edge Blend and Fillet tools are used to taper the top triangular section of the arm into the rectangular housing that fits into the body.

## Safety Validation

The peak stress of 21.16 MPa is below the PC-GF yield strength. Stresses along the majority of the arm span are substantially lower.

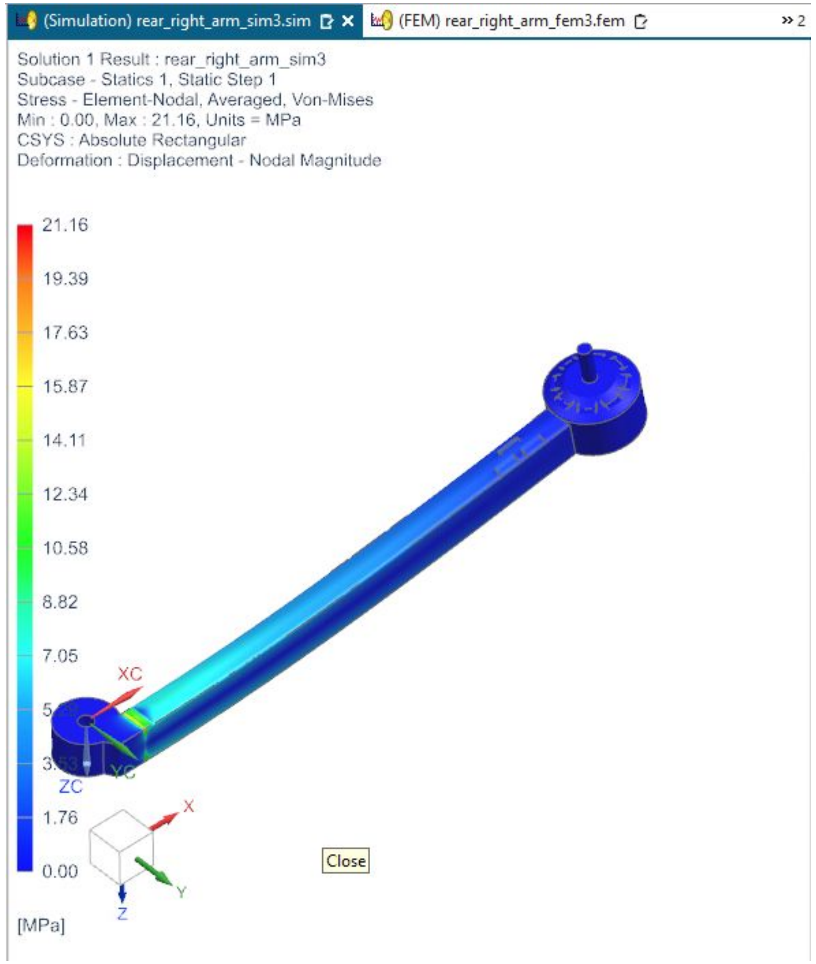


*Figure 12: Stress distribution under 5.6 N load*

# Propeller FEA Setup

## Design

Chord–camber ratio: ≈ 60:1 (48 mm chord, ~0.8 mm camber), indicating a low-camber blade optimized for small-scale, low-Reynolds-number operation.

Aerodynamic implication: Modest camber provides sufficient lift (thrust) without large pitching moments, supporting stable high-RPM performance and reduced root bending loads.

Structural tradeoff: Low camber limits unnecessary material and mass while preserving stiffness through chord length, yielding a favorable stiffness-to-mass ratio for a lightweight propeller.

## Loading Environment

Constraints: Center bore constrained axially, with the top hub surface fixed to model propeller cap clamping.

Loading: Averaged surface force applied over the blade to represent distributed aerodynamic thrust.

Intent: The averaged surface load is a distributed traction meant to approximate the net aerodynamic pressure on the blade (more realistic than a point force for thrust loading).

## Complexities

Creating the mesh and loading the blade involved manipulating airfoil geometry

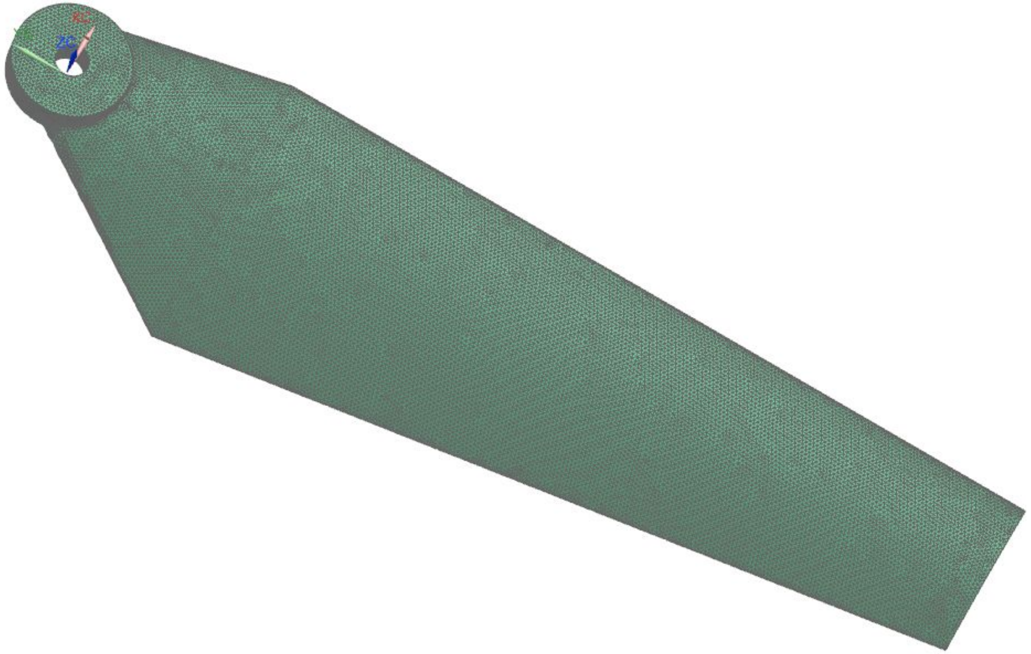

*Figure 13: Propeller Component Selected for Analysis*

# Propeller Mesh Convergence

### Convergence Conclusion

**Displacement convergence:** Max tip displacement changes **3.63 → 3.69 → 3.77 mm**, corresponding to **~2.12% change between the two finest meshes** and **~3.71% total change**, indicating the global stiffness response is likely converging..

**Stress trend:** Unaveraged stress increases **84.18 → 109.77 → 128.92 MPa** (**~14.85% between the two finest meshes**, **~34.70% total**), while averaged stress increases **66.86 → 80.01 → 89.72 MPa** (**~10.82% finest-mesh change**, **~25.48% total**).

**Interpretation:** The smooth increase with decreasing slope indicates stress is **approaching convergence but not fully converged**, whereas displacement is converged; stress results should therefore be treated as **conservative** unless further (local) refinement is performed.

| Ele Size (mm) | No. of Ele | No. of Nodes | Max Disp | unAve Stress | Ave Stress | Delta unAve | Delta Ave |
|---|---|---|---|---|---|---|---|
| 5.00 | 6683 | 12783 | 0.0144 | 26.64 | 25.07 | 7.5 | 5.5 |
| 3.00 | 16581 | 29183 | 0.0145 | 34.14 | 30.57 | -0.23 | -0.02 |
| 0.75/1.5 | 32304 | 54663 | 0.0146 | 33.91 | 30.55 | | |

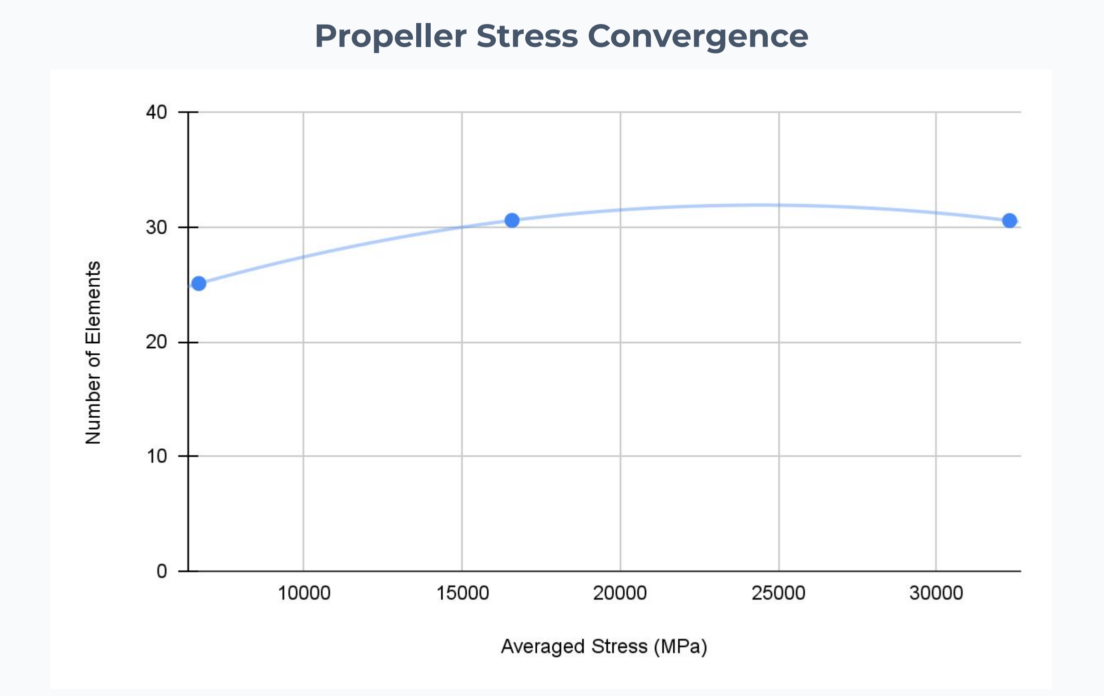

DISPLACEMENT AND STRESS ANALYSIS

# Propeller FEA Results

## Displacement Contour

ELASTIC DEFORMATION

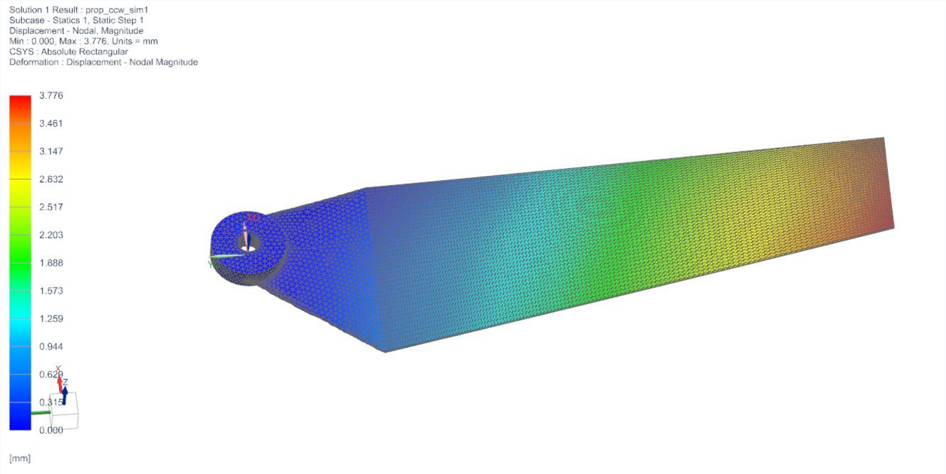


Total displacement field under maximum thrust load. The blades exhibit cantilever bending behavior with peak deflection occurring at the tips. The magnitude remains well within the small-displacement assumption, verifying stiffness requirements.

## Von Mises Stress

AVERAGED LOADS

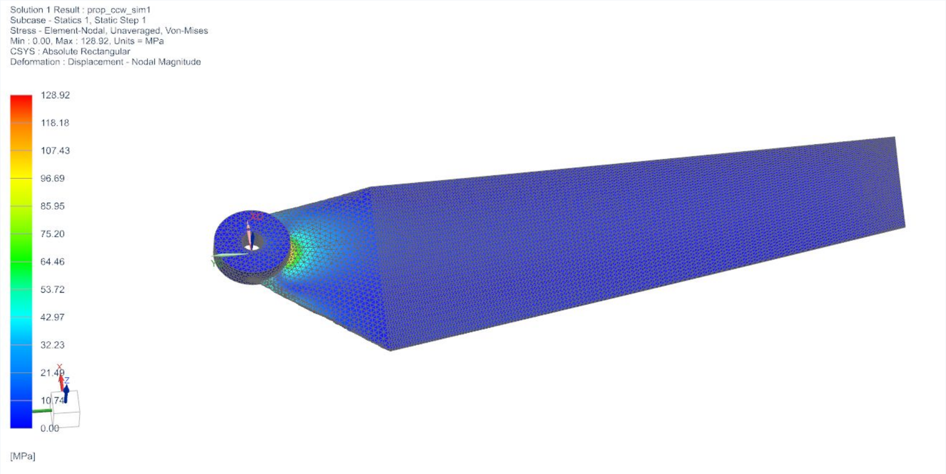


Von Mises stress distribution. Stress concentrations are localized at the root fillet where the blade joins the hub, which is the expected failure point. The peak stress values are below the yield strength of the PC-GF material, confirming a safety factor > 1.5.

DYNAMIC BEHAVIOR DEMONSTRATION

# Kinetic Simulation

## Camera Dynamics

KINEMATIC CHECK

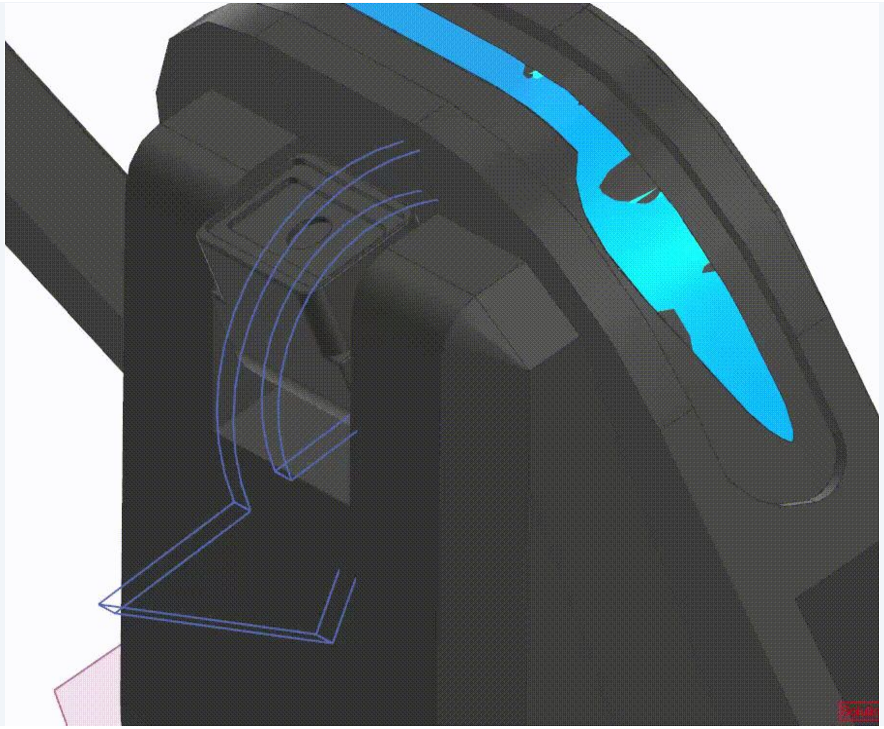

## Rotor Motion Analysis

MOTION VALIDATED

PATH TO PRODUCTION AND OPTIMIZATION

# Future Improvements

## Manufacturing Optimization

### Injection Molding Transition

Transition from additive manufacturing to scalable injection molding. Optimization includes consistent thin-wall sections (1.2–1.6 mm), uniform rib thickness ratios (~0.6× wall), and proper draft angles (1–2°) to reduce tooling wear and allow easy unmolding.

### Material Properties

Molding allows full realization of material properties. Molded ABS-GF exhibits higher strength and more predictable shrinkage, significantly improving clip retention and integrity for assembly.

## Future FEA Trials

### Propeller Geometry

Small-scale propellers operate at low Reynolds numbers, where simplified cambered sections (rather than classical NACA airfoils) are common; aerodynamic loading is therefore represented as an equivalent distributed pressure suitable for structural analysis.

### Propeller FEA

Improved FEA fidelity: Higher-fidelity models would incorporate a non-uniform pressure distribution and centrifugal stiffening, capturing spanwise load variation, torsion, and root stress concentrations beyond the beam-based approximation.

LITERATURE AND OTHER MATERIAL

# References


- Principles of Helicopter Aerodynamics, J. G. Leishman, Cambridge University Press
- Helicopter Theory, Wayne Johnson, Princeton University Press
- Quadrotor Dynamics and Control, G. Hoffmann et al., Springer
- Modelling and Control of Quadrotor Robots, P. Pounds et al., ACRA Proceedings
- Towards Dynamically-Favourable Quad-Rotor UAVs, P. Pounds et al., IEEE/RSJ IROS
- Rankine, W. J. M., “On the Mechanical Principles of Propellers,” Transactions of the Royal Institution of Naval Architects, 1865
- Froude, R. E., “On the Part Played in Propulsion by Differences of Fluid Pressure,” Transactions of the Institution of Naval Architects
- Cantrell, J. T. et al., “Experimental Characterization of the Mechanical Properties of 3D-Printed ABS and PC Parts,” Rapid Prototyping Journal
- Tymrak, B. M., Kreiger, M., Pearce, J. M., “Mechanical Properties of Components Fabricated with Open-Source 3-D Printers,” Materials & Design
- Ahn, S. H. et al., “Anisotropic Material Properties of Fused Deposition Modeling ABS,” Rapid Prototyping Journal
- Somireddy, M., Czekanski, A., “Anisotropic Mechanical Behavior of 3D Printed Composite Structures,” Materials & Design
- Garzón-Hernández, S. et al., “Design of FDM 3D Printed Polymers: An Experimental-Modelling Methodology,” Materials & Design
- ASTM D638, Standard Test Method for Tensile Properties of Plastics
- ASTM D790, Standard Test Methods for Flexural Properties of Plastics